Available online at www.sciencedirect.com
SCIENCE DIRECT®
Physica B 357 (2005) 193–198
PHYSICA B
www.elsevier.com/locate/physb

Dispersion of fullerenes in phospholipid bilayers and the subsequent phase changes in the host bilayers

U-Ser Jeng[a,*], Chia-Hung Hsu[a], Tsang-Lang Lin[b], Ching-Mao Wu[c], Hsin-Lung Chen[c], Lin-Ai Tai[d], Kuo-Chu Hwang[d]

[a]*National Synchrotron Radiation Research Center, Hsinchu 30077, Taiwan*
[b]*Department of Engineering and System Science, National Tsing Hua University, Hsinchu 30013, Taiwan*
[c]*Department of Chemical Engineering, National Tsing Hua University, Hsinchu 30013, Taiwan*
[d]*Department of Chemistry, National Tsing Hua University, Hsinchu 30013, Taiwan*

Abstract

We have studied the structure and phase transition characteristics of the fullerenes (C_{60})-embedded lipid bilayers. With small-angle neutron scattering (SANS), we have observed a degradation of bilayer ordering and a suppression effect on the phase transitions of the host vesicle bilayers of dipalmitoylphosphatidylcholine (DPPC), due to the embedment of fullerenes. The fullerene-embedded lipid system with substrate-oriented bilayers is also investigated using X-ray reflectivity and grazing incident small-angle X-ray scattering (GISAXS). In the depth direction, the multilamellar peaks observed in the X-ray reflectivity profile for the oriented DPPC/C_{60} bilayers reveal a larger head-to-head distance D_{HH} of 50.6 Å and a bilayer spacing D of 59.8 Å, compared to the $D_{HH} = 47.7$ Å and $D = 59.5$ Å for a pure DPPC membrane measured at the same conditions. Furthermore, the lipid head layers and water layers in the extracted electron density profile for the complex system are highly smeared, implying a fluctuating or corrugated structure in this zone. Correspondingly, GISAXS for the oriented DPPC/C_{60} membrane reveals stronger diffuse scatterings along the membrane plane than that for the pure DPPC system, indicating a higher in-plane correlation associated with the embedded fullerenes.

PACS: 61.10.Kw; 87.15.Ya; 87.16.Dg

Keywords: Fullerene; Phospholipid bilayers; SANS; GISAXS

1. Introduction

Recently, there are interests in fullerene-embedded lipid bilayers due to the attractions of the

*Corresponding author.
E-mail address: usjeng@nsrrc.org.tw (U-S. Jeng).

0921-4526/$ - see front matter © 2004 Elsevier B.V. All rights reserved.
doi:10.1016/j.physb.2004.11.055

electrochemical properties of fullerenes in lipids and the possible microenvironment for functionalizing fullerenes [1]. It has also been demonstrated that the embedded fullerenes can transport electrons efficiently across the host lipid membranes, which has a potential application in molecular electronics [2]. Further studies showed that the fast and efficient charge transport across a lipid-bilayer membrane was electronically mediated by fullerene aggregates [3]. We are particularly interested in the corresponding structure of fullerenes that mediates the transportation of electrons across lipid-bilayer membranes. In this report, we study the structural characteristics of fullerene-embedded phospholipids bilayers using small-angle neutron scattering (SANS), X-ray reflectivity, and grazing-incident small-angle X-ray scattering (GISAXS).

2. Experimental section

A $CS_2/CHCl_3$ solution of 20 mg/ml of dipalmitoylphosphatidylcholine (DPPC, molecular weight $M_w = 734$ g/mol) and 0.4 mg/ml of C_{60} was prepared as a mother solution for processing vesicle and oriented bilayer samples of DPPC/C_{60}. For vesicle samples, the mother solution was dipped and dried on the glass wall of a bottle for forming DPPC/C_{60} bilayers. After evaporation of solvent, D_2O was added into the bottle for a solution of 10 mM DPPC and 0.2 mM C_{60}. Instead of regular water, D_2O was used for increasing the scattering contrast between the solvent and the lipid vesicles in SANS [4]. The sample solution was subsequently treated with sonication for forming DPPC/C_{60} vesicles. In preparing a sample of oriented bilayers for X-ray reflection and GISAXS measurements, we first dipped the mother solution on a quartz plate of an area of 4 cm × 11 cm. After evaporation of organic solvent, the sample film of ~6 μm thick was sealed inside a box with a water reservoir. We used regular water, since X-ray scattered by electrons is insensitive to the isotope difference in regular water and D_2O. The sample was then annealed at temperatures interchanged between 20 °C and 50 °C for couple hours. For comparison, we also prepared vesicle bilayers and oriented bilayers of pure DPPC, using the same procedure.

SANS measurements were conducted for the vesicle samples on the 8-m SANS instrument at the National Institute of Standards and Technology (NIST), USA. Standard data reduction procedure was used for obtaining scattering cross-section per unit sample volume $I(Q)$ of the samples, with $Q = (4\pi/\lambda)\sin\theta$ defined by the scattering angle θ and the wavelength λ (6 Å used) [5]. X-ray reflection and GISAXS were conducted on a setup basing on an 8-circle diffractometer installed at the wiggler beamline BL17B in the National Synchrotron Radiation Research Center (NSRRC), Taiwan. The beam size used was $0.4 \times 0.4\,mm^2$, and the wavelength of the beam was 1.55 Å. The photon flux at the sample position was around 10^9 photons/s. The detailed setup for GISAXS was reported previously [6]. Samples were measured at an ambient environment of ~28 °C and ~50% relative humidity.

3. Results and discussion

3.1. SANS result

Fig. 1a shows the SANS profiles measured for the pure DPPC vesicle solution at 30, 40, and 50 °C, corresponding to the gel, ripple, and liquid crystal (LC) phases of the DPPC multilamellar vesicles [7,8]. The shifting of the Bragg peak position Q_p (around 0.1 $Å^{-1}$) of the lipid bilayers indicates that the bilayer spacing, $D = 2\pi/Q_p$, swells from 64 Å of the gel phase to 69 Å of the ripple phase, and then shrinks back to 65 Å of the LC phase, during the temperature changes [9,10]. At 40 °C the additional shoulder peak at $Q = 0.05\,Å^{-1}$, corresponding to an ordering length of ~125 Å [11], characterizes the additional in-plane ordering of the ripple phase of DPPC bilayers.

In contrast, the SANS profiles measured (Fig. 1b) for the DPPC/C_{60} vesicle solution at the same temperatures exhibit highly damped bilayer Bragg peaks for all the three temperatures, due to, presumably, the intercalation of C_{60} in the DPPC bilayers. At 50 °C (LC phase), however, the

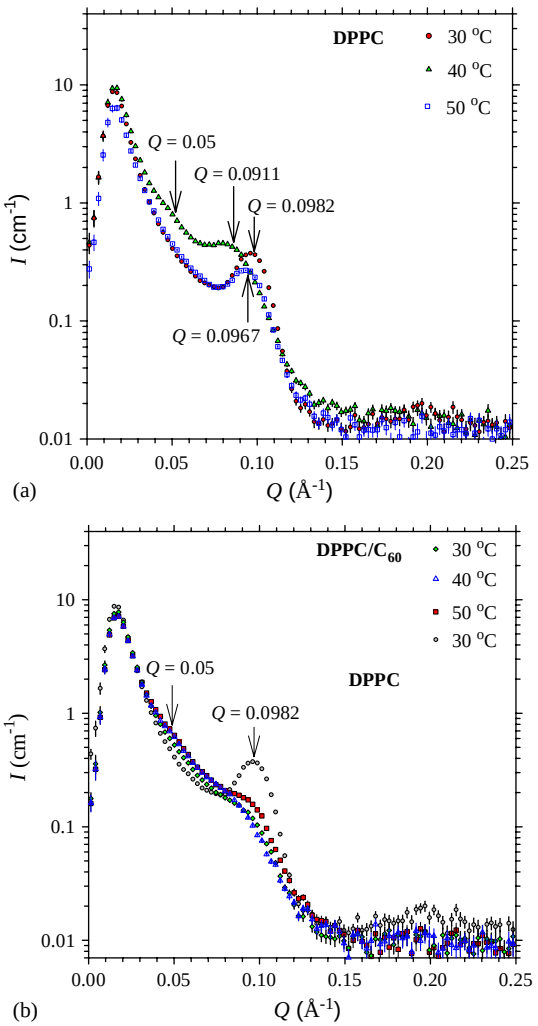

Fig. 1. (a) SANS profiles measured for the DPPC vesicles in D_2O at 30, 40, and 50 °C, corresponding to the gel, ripple, and LC phases of DPPC bilayers. The arrows indicate the corresponding Bragg peaks for each phase. (b) SANS profiles measured for the DPPC/C_{60} vesicles at the corresponding conditions for DPPC. The data for DPPC vesicles at 30 °C are shown for a comparison. The arrows at $Q = 0.05\,\text{Å}^{-1}$ and $Q \approx 0.1\,\text{Å}^{-1}$ indicate the in-plane and normal-to-plane orderings of the DPPC/C_{60} bilayers.

slightly sharper Bragg peak around $0.1\,\text{Å}^{-1}$, corresponding a better bilayer ordering, indicates that C_{60} can be better accommodated into the host bilayers in this phase of a larger interfacial area $A = 64\,\text{Å}^2$ per DPPC. For a comparison, A equals to $48\,\text{Å}^2$ in the gel and the ripple phases [12]. Furthermore, all the three SANS profiles measured for the DPPC/C_{60} vesicles at the three temperatures show broad bumps near $Q \sim 0.05\,\text{Å}^{-1}$. Compared to the ripple structure of DPPC observed, the result implies that the intercalation of C_{60} can trigger a ripple-like in-plane ordering in the DPPC bilayers. Unlike pure DPPC bilayers, the in-plane ordering of the complex system persists well at 50 °C. At even higher temperatures of 60 and 70 °C where the bilayer ordering peak at $Q \approx 0.1\,\text{Å}^{-1}$ fades, the broad scattering bump at $0.05\,\text{Å}^{-1}$ for in-plane ordering persists well (data not shown). This indicates that in-plane ordering triggered by C_{60} in the bilayers is of a mosaic nature rather than an origin of thermal fluctuations. The in-plane ripple-like ordering together with the deteriorated normal-to-plane ordering across the bilayers may facilitate the transportation of electrons across a lipid/C_{60} bilayer membrane, as mentioned in the beginning of the introduction. If this is the case, then, an analogous system would be the solid-state lithium polymer battery, where the PEO (polyethylene oxide)-based electrolyte conducts electrons drastically better when fluctuations of PEO chains are released from the dissociation of the PEO crystallization (packed structure) by lithium salts at low temperatures [13]. In the following, we use X-ray reflection and GISAXS to probe the depth and in-plane structures of a substrate-oriented DPPC/C_{60} membrane.

3.2. X-ray reflection and GISAXS

Fig. 2 shows the X-ray reflectivity data for the pure DPPC and the DPPC/C_{60} membranes. The presence of sharp Bragg peaks up to the sixth order for both films indicates highly oriented bilayers for both systems. From the Bragg peak positions, we deduce a bilayer spacing of 59.8 ± 0.3 Å for the DPPC/C_{60} system, which is slightly larger than 59.5 ± 0.3 Å for the pure DPPC system. The coherent stacking length estimated from the peak width is up to ~3500 Å or 58 bilayers out of the 1000 bilayers of the films (~6 μm). Compared to the 64 Å obtained previously from the DPPC vesicles in aqueous solutions at the gel phase, the smaller bilayer

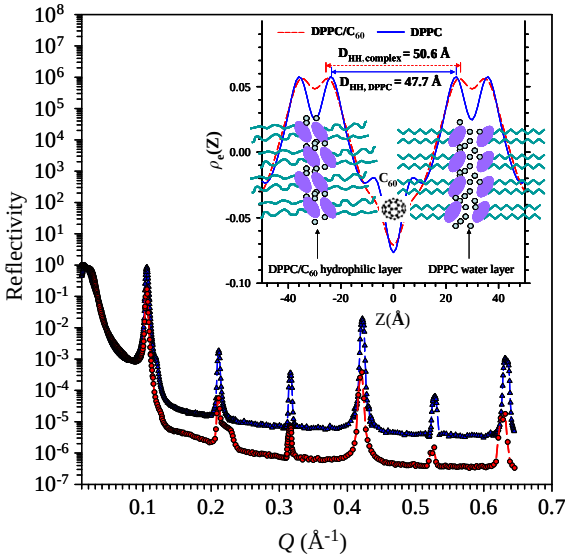

Fig. 2. X-ray reflectivity data for the DPPC and the DPPC/C_{60} multilamellar bilayers. The inset shows the relative electron density profiles $\rho_e(z)$ deduced from the reflectivity data. Cartoons for the C_{60} cage and the DPPC head layers and water layers of the pure (right-hand side) and complex (left-hand side) lipid systems are positioned according to the $\rho_e(z)$ profiles.

thickness obtained indicates that both oriented bilayers films are not fully hydrated. The 4 Å decrease in the bilayer thickness is likely due to the dehydration of the samples, which translates to a 60% hydration (close to the humidity of the measurement environment). For a fully hydrated DPPC bilayers, the thickness of water layer is 11 Å [10].

Due to the fine diffraction peaks observed, we reconstruct the one-dimensional electron density profiles (in the depth direction) for both the DPPC and the DPPC/C_{60} systems from the reflection data, using $\rho_e(z) \sim \sum_{k=1}^{n} \sqrt{I(Q_k)Q_k}\varphi_k \cos(Q_k z)$ with the same six-phase factors φ_k (--+---) for the six Bragg peaks observed in both systems. These phase factors for DPPC bilayers are well documented in literature [14,15]. In the Fourier transform for $\rho_e(z)$ from the integrated intensities $I(Q_k)$ of the six observed diffraction peaks, we have used a Lorentzian correction factor $1/Q$ for the oriented bilayers [16].

The inset of Fig. 2 shows the relative electron density profiles $\rho_e(z)$ and the corresponding molecular structures for the DPPC and the DPPC/C_{60} bilayers. The $\rho_e(z)$ profile obtained for the pure lipid system resembles that for fully hydrated DPPC bilayers [12,13]. However, the electron density corresponding to the water layer zone (see the inset of Fig. 2) is slightly higher than that for a pure water layer ($\rho_e(z) \sim 0$) [10,15]. We speculate that the higher $\rho_e(z)$ is a result of a density-averaged effect in the hydrophilic zone, where the two lipid head layers and the sandwiched water layer undergo collective undulations along the in-plane direction. Such undulations may be caused by a thinning of water layer (~7 Å) in the partially hydrated bilayers [17]. The undulation effect of the hydrophilic layers seems to be amplified drastically by the intercalation of C_{60}, since the dip in the $\rho_e(z)$ of the DPPC/C_{60} bilayers, corresponding to the water layer of low electron density, is now nearly smeared out completely (see the inset of Fig. 2). On the other hand, in the hydrophobic zone of $\rho_e(z)$, there are also small differences between the DPPC and DPPC/C_{60} systems. Likely, due to the accommodation of C_{60} (dia. ~10 Å) in the hydrophobic zone of DPPC bilayers (see the cartoon shown in Fig. 2), there is small-scaled chain reconfiguration which transforms the hydrophobic chains from the tight packing in gel phase to more a random or fluid-like packing. The fluid-like chains may in turn perturb the ordering in the hydrophilic zone for the smeared $\rho_e(z)$ observed. As a consequence, the lipid head-to-head distance $D_{HH} = 50.6$ Å extracted from $\rho_e(z)$ (see Fig. 2) is much larger than the 47.7 Å for the pure DPPC system.

In reconstructing the electron density profile for the DPPC/C_{60} system from the reflectivity data, we have neglected the side peak at $Q \sim 0.22$ Å^{-1} (Fig. 2) which is of a minor contribution to the integrated intensity for Fourier transform. The neglect of the side peak intensity does not change the major features of the reconstructed density profile nor our conclusions drawn from the electron density profile obtained. Nevertheless, the side peak indicates an additional ordering in the DPPC/C_{60} system. Since C_{60} has strong tendency in self aggregation, it is possible that the embedded C_{60} cages form C_{60}-rich (or aggregation) regions in the lipid bilayers, and create a local membrane thinning

effect [18] for the additional bilayer spacing observed. The weak intensity for the additional ordering may be due to the large molar ratio 50:1 between DPPC and C_{60}. Furthermore, X-ray reflectivity, probing only the depth density profile "averaged" over the lateral direction, is not sensitive to the local inhomogeneity. Complementarily, GISAXS, sensitive to local inhomogeneity, can reveal in-plane ordering structures better than X-ray reflectivity, as demonstrated below.

Using GISAXS with an incident angle, 0.225°, much smaller than the Bragg angle, we have observed highly asymmetrical scattering patterns for the well-oriented DPPC and DPPC/C_{60} bilayers. The pronounced diffuse Bragg peaks up to the third order observed for both DPPC/C_{60}- and DPPC-oriented bilayers, in the direction normal to the bilayer plane (z direction in Fig. 3a), copy the same bilayer spacing as that observed in the X-ray reflectivity. From the diffuse peak widths (Fig. 3b), we estimate that there are about 44 bilayers which undergo the collective normal-to-plane fluctuations (or corrugation) in both systems. The ordered bilayers are comparable to that obtained from the X-ray Bragg peak width. This result indicates that the two pure and complex lipid systems indeed consist of slightly misaligned microdomains, each has well-oriented bilayers (~50 bilayers) in its own microdomain [19,20]. The misalignment of the microdomains in the vertical direction leads to the GISAXS patterns of a mirror image of the X-ray reflectivity profiles measured previously. As a consequence, the additional ordering peaks, corresponding to a bilayer spacing of 48 Å, observed in the DPPC/C_{60} system are consistent with that in the X-ray reflectivity. In addition, we have also observed stronger diffuse scatterings in the in-plane direction of the DPPC/C_{60} bilayers, especially at the specular position ($Q_z = 0.0319\,\text{Å}^{-1}$, as indicated by dotted zone in Fig. 3a). With the Debye–Buche model [6], the in-plane correlation length estimated from the diffuse scattering for the DPPC/C_{60} bilayers is 76 Å, which is larger than the 52 Å for the DPPC bilayers (inset of Fig. 3b). The accuracy of the estimation, however, is interfered by the contribution of the powder ring scattering (Fig. 3a) from the bilayers of defect orientation in the system [17]. Nevertheless, the correlation length extracted

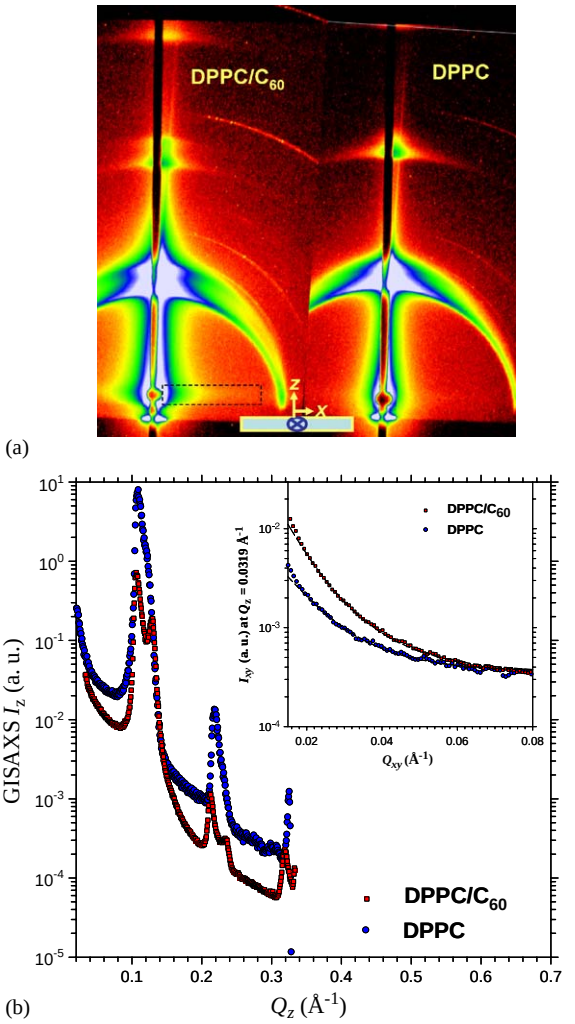

Fig. 3. (a) GISAXS images taken for the DPPC and DPPC/C_{60} multilamellar bilayers, with an incident angle of 0.225° (or $Q_z = 0.0319\,\text{Å}^{-1}$). At the bottom, the rectangle indicates the film orientation, with the cross for the beam incident direction. (b) The GISAXS profiles extracted from the IP images along the z direction (normal to the film plane) for the pure and complex systems. In the inset, the in-plane GISAXS profiles extracted at $Q_z = 0.0319\,\text{Å}^{-1}$, as indicated by the dotted box in (a), are fitted (dashed curves) using the Debye–Buche model.

for DPPC bilayers is reasonable, compared to that obtained by Liu et al. for a similar lipid bilayers of DOPC [16]. We speculate that the larger in-plane correlation for the DPPC/C_{60} bilayers obtained may relate to the aggregation of C_{60} along the hydrophobic planes of the lipid bilayers. Aggregation of

C_{60} in lipids bilayers was evidenced by Niu et al. in the photovoltage and photocurrent measurements for C_{60}-dopped membranes [3].

4. Conclusions

In this study, we show that the embedment of C_{60} in the vesicles of DPPC bilayers can suppress the phase transitions of the host lipid bilayers, and result in a deteriorated bilayer ordering across the lipid bilayers and an enhanced correlation along the bilayer planes. Similar structural characteristics are also observed in the oriented bilayers of DPPC/C_{60} using X-ray reflectivity and GISAXS. In the oriented bilayers, of much smaller thermal fluctuations compared to vesicle bilayers, we have found an additional ordering in the C_{60}-intercalated lipid membrane. The larger corrugated structure with a better in-plane correlation observed in C_{60}-embedded lipid membrane may associate with the suggested electron conductive path induced by C_{60} aggregates in lipid bilayres [3].

Acknowledgments

We thank the National Institute of Standards and Technology for the SANS beamtime.

References

[1] N. Nakashima, Y. Nonaka, T. Nakanishi, T. Sagara, H. Murakami, J. Phys. Chem. 102 (1998) 7238.
[2] K.C. Hwang, D. Mauzerall, Nature 361 (1993) 138.
[3] S. Niu, D. Mauzerall, J. Am. Chem. Soc. 118 (1996) 5791.
[4] S.H. Chen, T.L. Lin, in: K. Skod, D.L. Price (Eds.), Methods of Experimental Physics—Neutron Scattering in Condensed Matter Research, vol. 23B, Academic Press, New York, 1987 (Chapter 16).
[5] C.J. Glinka, J.G. Barker, B. Hammouda, S. Krueger, J.J. Moyer, W.J. Orts, J. Appl. Crystallogr. 31 (1998) 430.
[6] U. Jeng, T.-L. Lin, K. Shin, C.-H. Hsu, H.-Y. Lee, M.H. Wu, Z.A. Chi, M.C. Shih, L.Y. Chiang, Physica B 336 (2003) 204.
[7] P.C. Mason, B.D. Gaulin, R.M. Epand, G.D. Wignall, J.S. Lin, Phys. Rev. E 59 (1999) 3361.
[8] S.E. Feller, R.M. Venable, R.W. Pastor, Langmuir 13 (1997) 6555.
[9] J. Lemmich, K. Mortensen, J.H. Ipsen, T. Honger, R. Bauer, O.G. Mouritsen, Phys. Rev. E 53 (1996) 5169.
[10] D. Richter, D. Schneiders, M. Monkenbusch, L. Willner, L.J. Fetters, J.S. Huang, M. Lin, K. Mortensen, B. Farago, Macromolecules 30 (1997) 1053.
[11] J. Katsaras, S. Tristram-Nagle, Y. Liu, R.L. Headrick, E. Fontes, P.C. Mason, J. Nagle, Phys. Rev. E 61 (2000) 5668.
[12] J. Nagle, S. Tristram-Nagle, Biochim. Biophys. Acta 1469 (2000) 159.
[13] H.M. Kao, C.L. Chen, Angew. Chem. Int. Ed. 43 (2004) 980.
[14] C.-M. Wu, W. Liou, H.-L. Chen, T.-L. Lin, U. Jeng, Macromolecule 37 (2004) 4947.
[15] J.F. Nagle, R. Zhang, S. Tristram-Nagle, W. Sun, H.I. Petrache, R.M. Suter, Biophys. J. 70 (1996) 1419.
[16] T. Salditt, Curr. Opin. Struc. Biol. 13 (2003) 467.
[17] Y. Liu, J.F. Nagle, Phys. Rev. E 69 (2004) 040901.
[18] W.T. Heller, A.J. Waring, R.I. Lehrer, T.A. Harroun, T.M. Weiss, L. Yang, H.W. Huang, Biochemistry 39 (2000) 139.
[19] M. Vogel, C. Munster, W. Fenzl, D. Thiaudiere, T. Salditt, Physica B 283 (2000) 32.
[20] J.S. Gutmann, P. Muller-Buschbaum, D.W. Schubert, N. Stribeck, D. Smilgies, M. Stamm, Physica B 283 (2000) 40.